Atmospheric Research 285 (2023) 106626

Contents lists available at ScienceDirect

Atmospheric Research

journal homepage: www.elsevier.com/locate/atmosres

Variations of chemical composition of NR-PM_1 under the influence of sea land breeze in a coastal city of Southeast China

Yuping Chen [a,b,c], Chen Yang [a,b,c], Lingling Xu [a,b,*], Xiaolong Fan [a,b], Jiayan Shi [b], Ronghua Zheng [a,b], Youwei Hong [a,b], Mengren Li [a,b], Taotao Liu [a,b,c], Gaojie Chen [a,b,c], Liqian Yin [a,b], Jinsheng Chen [a,b,*]

[a] Center for Excellence in Regional Atmospheric Environment, Institute of Urban Environment, Chinese Academy of Sciences, Xiamen 361021, China
[b] Key Lab of Urban Environment and Health, Institute of Urban Environment, Chinese Academy of Sciences, Xiamen 361021, China
[c] University of Chinese Academy of Sciences, Beijing 100049, China

ARTICLE INFO

Keywords:
Sea Land Breeze (SLB)
Meteorology
Secondary aerosol
Photochemical reaction
Coastal city

ABSTRACT

Sea land breeze (SLB) is a common local mesoscale circulation in coastal areas, which varies local weather conditions and further affects the diffusion and transport of air pollutants. This study investigated the variation of meteorological conditions, air pollutants concentrations, and aerosol chemical composition under the influence of SLB circulation in a coastal city of Southeast China during Nov. 1 – Dec. 31, 2020, when SLB circulation frequently occurred. The day-night difference in meteorological parameters was amplified on SLB days with a marked daytime peak of *T* and UV while the nighttime pronounced minimum boundary layer height compared to non-SLB days. The average mass concentrations of NR-PM_1 (non-refractory submicron particles) measured by a Q-ACSM were 9.6 ± 6.5 μg m^{-3} on SLB days and 11.6 ± 7.3 μg m^{-3} on non-SLB days, but the NR-PM_1, as well as gaseous pollutants like NO_2 on SLB days, showed a marked peak in the late evening. The NR-PM_1 on SLB days was characterized by a high fraction of organic aerosol (OA). Moreover, the NR-PM_1 showed a significant increase of more-oxidized OOA (MO-OOA) during the sea breeze period, which was associated with enhanced photochemical reactions due to strong UV and elevated O_x. Comparison between a SLB case and a local pollution case further highlighted the elevated contribution of OOA to NR-PM_1 and the cyclic amplification of air pollutants in SLB conditions. Our study enhances the understanding of the influence of SLB on air pollutants and aerosol chemical composition and provide a plausible explanation for the atmospheric pollution processes in coastal cities.

1. Introduction

Aerosols have both direct and indirect effects on global climate (Bellouin et al., 2020; Cohen et al., 2017; Paasonen et al., 2013) and have drawn wide attention in the past few decades owing to its effects on air quality (Lelieveld et al., 2015). Furthermore, aerosols, especially submicron aerosols, are harmful to human health (Shiraiwa et al., 2017). The loading of aerosol present in the atmosphere is directly related to the simultaneous primary and secondary aerosol precursor emissions from multiple sources, secondary aerosol formation rates, removal processes (e.g., sedimentation and precipitation scavenging), and the synergies of local meteorological conditions and regional transport (An et al., 2019; Hu et al., 2017; Sun et al., 2016).

Sea land breeze (SLB) is a local mesoscale topographical circulation unique to the atmospheric boundary layer in coastal areas. The study of SLB first began in the 1920s when Jeffreys put forward the theory of the generation of SLB (Jeffreys, 1922). SLB not only affects local weather variations but sometimes also triggers strong convective weather such as thunderstorms, strong winds, and short-term heavy precipitation along the sea breeze front, which affects the diffusion and transport of air pollutants in the region (Ding et al., 2004; Liu and Chan, 2002; Miao and Yang, 2020). SLB circulation is a wind system that varies within a natural day. The temperature of land is higher than that from the sea during the day, and it is reverse at night, resulting in the circulation characteristics of sea breeze (SB) during the day and land breeze (LB) at night. The LB typically begins at midnight and continues until after sunrise,

* Corresponding authors at: Center for Excellence in Regional Atmospheric Environment, Institute of Urban Environment, Chinese Academy of Sciences, Xiamen 361021, China
E-mail addresses: linglingxu@iue.ac.cn (L. Xu), jschen@iue.ac.cn (J. Chen).

https://doi.org/10.1016/j.atmosres.2023.106626
Received 19 July 2022; Received in revised form 14 January 2023; Accepted 14 January 2023
Available online 18 January 2023

resulting in the urban air masses being transported to the marine in darkness for several hours (Cass and Shair, 1984).

The temperature inversion formed by the encounter of coastal land-sea air currents is an important unfavorable meteorological condition leading to particulate matter pollution, which inhibits vertical movement and transport of air due to the lack of thermal convection and sustained stable stratification (Yang et al., 2022). What's more, the pollutants accumulation of the same air mass repeating across the observation site due to the daily LB/SB reversals probably results in high aerosol concentrations and enhanced contributions of aging components (Cass and Shair, 1984; Lo et al., 2006). Nocturnal chemical transformations are probably important in determining the overall impact of LB on air quality, especially considering that the products of nocturnal reactions are blown back inland by SB during the following day (Wagner et al., 2012). Augustin et al. (2020) pointed out that the SLB circulations provide favorable conditions for secondary aerosol (SA) formation, such as temperature/humidity fluctuations, boundary layer circulation, and relatively high concentrations of various precursors. Previous studies have often applied a theoretical approach using analytical and numerical modeling to study the physical processes responsible for the SLB development and the spatiotemporal distribution of pollutants (Liu et al., 2022; Miller et al., 2003; Papanastasiou and Melas, 2009; Tsai et al., 2011). However, field observations about the variation of aerosol chemical composition under the influence of SLB are still limited (Di Bernardino et al., 2021).

Here, the study on the influence of SLB circulations on air pollutants, as well as aerosols and its chemical composition was conducted in Xiamen, a coastal city of Southeast China, where SLB commonly occurs. The average number (percentage) of SLB days was 60 (14.5–20.8%) per year during the period 2017–2020, which frequently presented in autumn and winter season (Fig. S1). Meteorological parameters, conventional air pollutants, and the chemical composition of NR-PM_1 (non-refractory submicron particles) were simultaneously observed during the period with frequent SLB occurrence and high aerosol concentrations. The main objectives of this study were to (1) reveal the variations of meteorology and conventional pollutants from non-SLB to SLB days, (2) characterize the NR-PM_1 and its chemical composition on SLB days and non-SLB days, and (3) investigate the evolution of air pollutants and aerosol chemical composition during the SLB process.

2. Experimental methods

2.1. Overview of field observations

Xiamen is located on the west coast of the Taiwan Strait (Fig. 1) and is a subtropical city with a warm climate and high relative humidity throughout the year. The observation period in this study was from Nov. 1 to Dec. 31, 2020, when the SLB phenomenon frequently occurred. Two days (Nov. 5–6) were excluded for instrument malfunction.

The field measurements were conducted at the Institute of Urban Environment (IUE), Chinese Academy of Sciences (118°03′E, 24°36′N) in Jimei District of Xiamen city. IUE is a suburban site close to Jimei Avenue and Haixiang Avenue with high traffic flow (~100 m away). Industrial point sources mainly distributed to the northeast and the southwest of the study site (> 5 km away). The IUE site was located approximately 17 km off the southeast coast of China. The instruments were deployed on the top of the 80 m building at the IUE site.

2.2. Observation instruments

The chemical composition of NR-PM_1, including organics aerosol (OA), nitrate (NO_3), sulfate (SO_4), ammonium (NH_4), and chloride (Cl), was measured by an ACSM. The detail of ACSM instrument operation and calibration can be found in previous studies (Ng et al., 2011; Sun et al., 2012; Chen et al., 2022). The ionization efficiency (IE) was 4.27 × 10^{-11} and relative ionization efficiency (RIE) for ammonium and sulfate

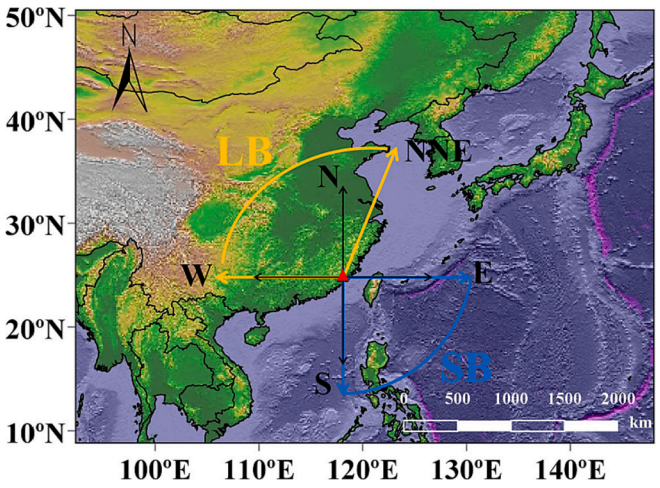

Fig. 1. Location of Xiamen (red triangle) in China. The sea breeze (SB) is blowing from the east-south (*E*-S), and the land breeze (LB) is blowing from the west-north-northeast (W-N-NNE). (For interpretation of the references to colour in this figure legend, the reader is referred to the web version of this article.)

was 5.49 and 0.53, respectively. The default RIE values were used for nitrate (1.1), OA (1.4), and chloride (1.3) (Canagaratna et al., 2007; Ng et al., 2011).

Trace gases O_3, NO_x, CO, and SO_2 were simultaneously measured by Thermo Fisher 49*i*, 42*i*, 48*i*, and 43*i*, respectively (Thermo Fisher Scientific, Waltham, MA, USA). Those instruments were regularly calibrated and maintained to keep well operational status and data quality. Meteorological parameters, i.e., wind speed (WS), wind direction (WD), temperature (*T*), relative humidity (RH), and pressure (P), were recorded from an automatic weather station of Xiamen, about 0.9 km far away from IUE. Ultraviolet radiation (UV) was determined by a UV radiometer (KIPP & ZONEN, SUV5 Smart UV Radiometer). Boundary layer height (BLH) was obtained from the European Centre for Medium-Range Weather Forecasts (ECMWF) reanalysis (https://www.ecmwf.int).

2.3. Identification of OA factors

The data of ACSM was analyzed with the standard Wave Metrics Igor Pro based data analysis software (version 6.37). The data analysis protocols were referred to the previous studies (Sun et al., 2012; Wang et al., 2017). The collection efficiency (CE) values were calculated using algorithms described by Middlebrook et al. (2012). The yielded composition-dependent CEs (0.51 ± 0.07) were comparable to the empirical CE of 0.5. In this study, we adopted the CE empirical value of 0.5, which has been widely used in field observations (Sun et al., 2015; Xu et al., 2017; Zhao et al., 2017; Zhao et al., 2020).

Five OA factors including HOA (hydrocarbon-like OA), BBOA (biomass burning OA), CCOA (coal combustion OA), LO-OOA (less-oxidized oxygenated OA), and MO-OOA (more-oxidized oxygenated OA), were identified by SoFi (version 6.G) along with the multi-linear engine (ME-2) algorithm (Canonaco et al., 2013). In this study, we used the spectra profile of HOA and BBOA derived from standard spectra as constraints to analyze the source of organic matrices during the whole observation period (Ng et al., 2011), and other factors were not constrained. The constraint value (a-value) was selected from 0 to 1 with 0.1 as an interval. Note that the average spectra with constraint values of 0, 0.1, and 0.2 are used for analysis in this study.

The mass spectral and identification of OA factors are presented in SI (Fig. S2). Specifically, CCOA was mixed with COA (cooking OA) due to the strong correlation between CCOA and COA fragments ($r = 0.96$ for m/z 55 and $r = 0.68$ for m/z 98). The distinction between LO-OOA and MO-OOA is their degree of oxidation (Xu et al., 2017), and the fraction

of *m/z* 43 was larger for LO-OOA than MO-OOA. Consistent with the lower degree of oxidation for LO-OOA, its correlations with hydrocarbon-like ions (e.g., $C_nH^+_{2n+1}$ and $C_nH^+_{2n-1}$) were stronger than those for MO-OOA. In addition, LO-OOA correlated well with both cooking and combustion fragments, indicating that LO-OOA contained high levels of freshly emitted species (Hu et al., 2016).

3. Results and discussion

3.1. Identification of sea land breeze (SLB)

Sea land breeze is a mesoscale local circulation in the lower atmosphere caused by the difference in the thermal properties of land and sea (Masselink and Pattiaratchi, 1998). The identification and definition of SLB are not consistent at different sites, depending on the local weather conditions and the background synoptic winds (Gahmberg et al., 2010). Differences in latitude, coastline shape, and coastal topography lead to SLB with commonalities and local characteristics in different regions (Borne et al., 1998). In this study, the coastline is characterized by a northeast-southwest trend. The sea breeze (SB) is blowing from the east-south (*E*-S), and the land breeze (LB) is blowing from the west-north-northeast (W-N-NNE). Still winds (wind speed <0.2 m s^{-1}) are neither sea breezes nor land breezes.

According to the observed wind direction, we firstly divided a natural day into four periods. Specifically, 01:00–08:00 LT is the LB period, 13:00–20:00 LT is the SB period, and 9:00–12:00 LT and 21:00–24:00 LT are the LB and SB transition periods. As shown in the workflow (Fig. S3), the days met with the following conditions were counted as SLB days: (1) The 24-h average ground wind speed is below 10 m s^{-1}, (2) During the LB period, the occurrence hour of land breeze is $\geq$4 h, and the occurrence hour of sea breeze is $\leq$2 h, and (3) During the SB period, the occurrence hour of sea breeze is $\geq$4 h, and the occurrence hour of land breeze is $\leq$2 h.

Based on the above method, a total of 11 SLB days (Fig. 2, pink area marked) were identified from November to December 2020. Other days were classified as non-SLB days. Meteorological parameters such as wind speed, wind direction, and boundary layer height that differed from non-SLB days to SLB days probably affect variations in gaseous pollutants and aerosol chemical composition, which would be discussed in detail later.

3.2. Variations of meteorology and conventional pollutants

Relevant studies have shown that the sea-land temperature difference is the major factor driving SLB phenomenon. The larger the temperature difference between land and sea, the stronger the development trend of SLB (Furberg et al., 2002). Consistently, the diurnal variations of temperature showed a larger daytime and nighttime difference on SLB days than on non-SLB days (Fig. 3e). There was little difference in average RH between SLB and non-SLB days (Table S1). However, when wind was transitioning to SB after 13:00, the RH on SLB days remarkably increased compared to non-SLB days, indicating that the SB carried sufficient water vapor. High RH at night during SLB days had a potential effect on the aqueous-phase secondary aerosol formation (Wang et al., 2017; Xu et al., 2017).

The parameters related to photochemical reaction, such as UV and O_x ($O_3 + NO_2$) were also higher on SLB days than non-SLB days, especially for the daytime (Fig. 3d). The peaked *T* and UV during the daytime would be conducive to promote the process of chemical reactions (Chen et al., 2021; Zhou et al., 2020). Although the average mixing ratio of O_3 was slightly lower on SLB days, the diurnal variations showed that the O_3 mixing ratio during the daytime was higher on SLB days than non-SLB days (Fig. 3f). While, the major source of O_3 is photochemical reaction formation and transport (Huang et al., 2006; Zhao et al., 2016). The marked O_3 peak at midday during SLB days was likely resulted from the enhanced photochemical formations due to the higher UV. When the intensity of photochemical reactions weakened, the O_3 mixing ratio decreased more slowly on non-SLB days compared to SLB days, which

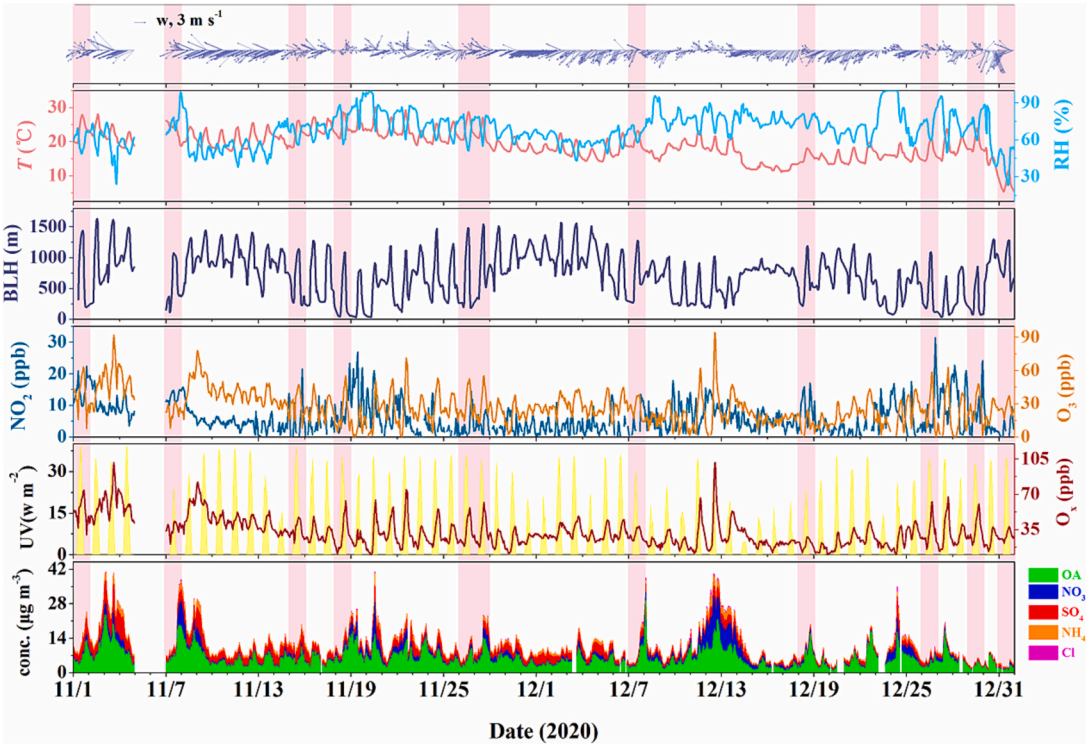

Fig. 2. Temporal variations of meteorological parameters, gaseous pollutants, and chemical composition (OA: organic aerosol, NO_3: nitrate, SO_4: sulfate, NH_4: ammonium, and Cl: chloride) in NR-PM_1 during the observation period. The pink area is the day of the sea land breeze (SLB) days. (For interpretation of the references to colour in this figure legend, the reader is referred to the web version of this article.)

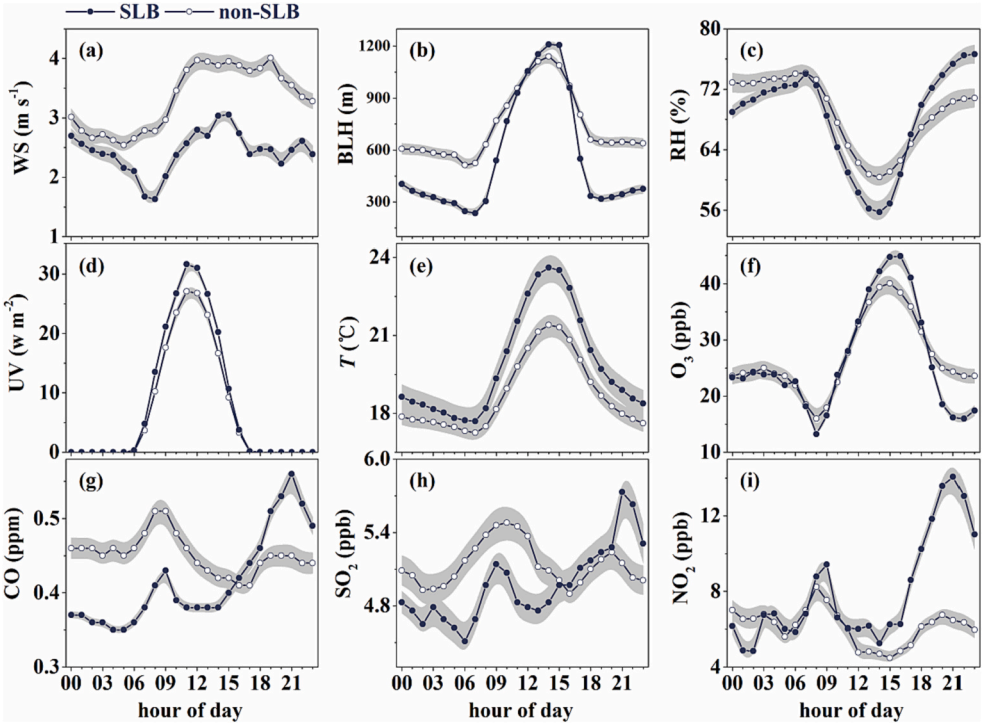

Fig. 3. Average diurnal variations of meteorological parameters ((a) WS, (b) BLH, (c) RH, (d) UV, (e) T) and mixing ratios of gaseous pollutants ((f) O_3, (g) CO, (h) SO_2, (i) NO_2) during SLB (solid point) and non-SLB (hollow point) days. Note: The error bar value is one-tenth of the original value.

could be attributed to the effect of a stronger transport on non-SLB days (Fig. S4). O_x was proven to be a robust indicator of atmospheric oxidation capacity (Herndon et al., 2008; Xu et al., 2017). We expected that combined the more favorable meteorology (high UV) and enhanced oxidation capacity (elevated O_x) on SLB days would have significant effect on the photochemical formations of secondary components, like NO_3, SO_4, and OOA (Sun et al., 2016; Yang et al., 2020; Xu et al., 2017).

Among the observed meteorological parameters, the BLH and WS showed the most remarkable differences between SLB and non-SLB days (Table S1). The average BLH and WS were 560 ± 394 m and 2.44 ± 1.12 m s^{-1} on SLB days relative to 743 ± 353 m and 3.33 ± 1.42 m s^{-1} on non-SLB days, respectively. The lower BLH and WS during SLB days were not conducive to the diffusion of pollutants. Accordingly, the mixing ratio of NO_2, which is mainly emitted from local traffic and industries, increased during SLB periods. The gaseous pollutants like CO, SO_2, and NO_2 (Fig. 3g, h, i) during non-SLB days showed a bimodal peak in the morning and evening rush hours. In contrast, the concentration of those pollutants during SLB days increased rapidly from the late afternoon with the remarkable evening peak. The BLH decreased rapidly in the afternoon during SLB days compared to non-SLB days (Fig. 3b). Thus, the late evening peak of pollutants on SLB days was likely a combined effect of pollutant emissions during the evening rush hours and the rapid decline of BLH. Another possible reason was that the contaminants being carried to the ocean by the LB would be brought back to land by the developed SB, which could contribute to the late evening peaks of gaseous pollutants during SLB days.

3.3. Variations of NR-PM_1 and chemical composition

3.3.1. Comparison of NR-PM_1 on SLB and non-SLB days

The average mass concentrations of NR-PM_1 on SLB and non-SLB days were 9.6 ± 6.5 μg m^{-3} and 11.6 ± 7.3 μg m^{-3}, respectively. There was 16.5% lower on SLB than on non-SLB days (Table S1). As shown in Fig. 4a, the diurnal variation trend of NR-PM_1 on non-SLB days was flat. In contrast, the concentration of NR-PM_1 during SLB days showed a low initial level in the early morning, increased continuously during the daytime and peaked in the late evening. On the one hand, when the LB was transformed into SB, the SB brought back the polluted

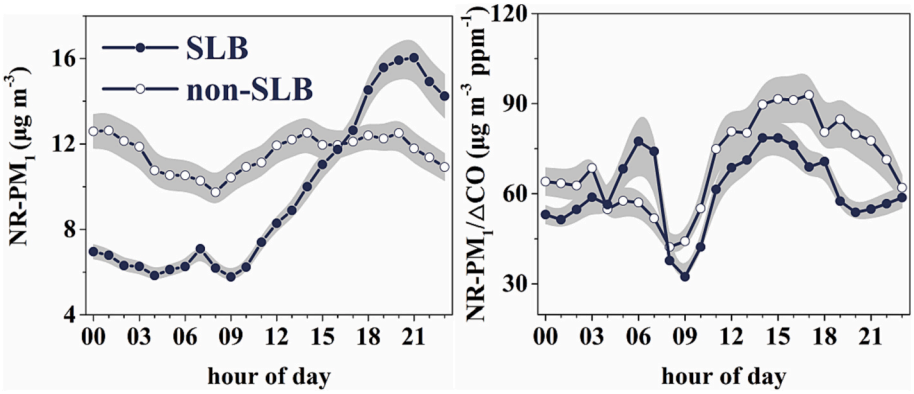

Fig. 4. Diurnal variations of NR-PM_1 mass concentrations (a) and NR-PM_1/ΔCO ratios (b) during SLB and non-SLB days.

air mass that blew to the ocean during the LB. Alternating LB and SB circulation allowed the air mass carrying pollutants to pass through the observation site multiple times. On the other hand, the shallow boundary layer in the evening (after 18:00, Fig. 3b) was expected to have a significant impact on pollutant accumulation. During the SB period, the stable over-water air mass advection onto land, the height of the boundary layer in coastal areas decreases significantly due to the formation of the thermal internal boundary layer (TIBL; Berman et al., 1999). TIBL made the atmospheric boundary layer more stably stratified and unfavorable diffusion of pollutants with strong sinking flowing (Yang et al., 2022). At this time, the downdraft air carries pollutants to the surface and inhibits the vertical diffusion of pollutants that continue to be emitted from the terrestrial surfaces. The redistribution of pollutants thus led to higher ground concentrations. In addition, studies have shown that low-level temperature inversion is prone to occur during the SB period, which inhibits the diffusion of pollutants (Yang et al., 2022). A previous study in Hong Kong, China, reported that the accumulation of local and regional pollutants was enhanced by slowing surface winds and a well-defined SLB establishment (Lee et al., 2013).

In this study, ΔCO was used to normalize the mass concentration of NR-PM_1 to deduct the effect of physical conditions such as the BLH and the partial effect of primary emissions. Different to absolute NR-PM_1 concentrations, the diurnal variation of NR-PM_1/ΔCO ratios was more similar between SLB and non-SLB (Fig. 4b). NR-PM_1/ΔCO ratios increased in the daytime likely due to the photochemical formation of aerosols. However, in the evening, the NR-PM_1/ΔCO ratios on non-SLB days showed a continuous downward trend, while the ratio on SLB days decreased to evening rush hours and then increased to a peak before sunrise. The increase in NR-PM_1/ΔCO ratios at night on SLB days was probably ascribed to the influence of nocturnal chemistry. Distinctly, the outstanding peak of NR-PM_1 concentrations in the evening (19:00–21:00) on SLB days was in contrast to the relatively low NR-PM_1/ΔCO ratios. The comparison indicates that the late evening peak of NR-PM_1 on SLB days was largely attributed to the collapse of the atmospheric boundary layer that favors the accumulation of pollutants.

3.3.2. Comparison of chemical composition on SLB and non-SLB days

In terms of the chemical composition of NR-PM_1, the concentrations of major chemical composition were basically lower on SLB days than non-SLB days, with the smallest change for OA (−7.2%), largest change for NO_3 (−36.9%), and moderate change for other composition (−23.8% – -20.7%) (Table S1). The chemical composition of NR-PM_1 was slightly different from SLB to non-SLB. The former had lower SIA (sulfate, nitrate, and ammonium) and higher OA fraction than the latter (Fig. S5). As shown in Fig. S6, the reduction of SO_4 fraction on SLB days evolved from late afternoon to evening. Sulfate is formed over a regional scale and is generally considered to be transportable over long distances (Shen et al., 2012; Zhou et al., 2020). SLB is a local mesoscale topographical circulation, thereby, the impact of transport on observation sites is relatively low on SLB days, which could explain the reduction of sulfate fraction on SLB days. The relatively low fraction of NO_3 on SLB days could be attributed to the rapid decomposition of NO_3 with higher temperatures and radiation (Seinfeld and Pandis, 2016; Sun et al., 2012).

The fractions of OA factors all increased to varying degrees on SLB days. The increased POA fraction (HOA, BBOA, and CCOA) demonstrated that the SLB phenomenon was in favor of the local accumulation of pollutants. The increase in OOA (LO-OOA and MO-OOA) was likely due to enhanced formation processes characterized by strong UV and atmospheric oxidation capacity during SLB days as mentioned above. A previous study conducted on Pearl River Delta (PRD) has observed an increase in O/C ratio on a SLB circulation, indicating a considerable rise in the oxidation degree of OA in this period (Lee et al., 2013). Additionally, the chemical composition of NR-PM_1 during the time period 19:00–21:00 of SLB days was characterized by a significant increase of HOA and NO_3 fractions (Fig. S6). HOA and NO_3 are the primary and converted pollutants mainly from traffic emissions. Simultaneously, the HOA/ΔCO ratio exhibited a peak during evening rush hours (Fig. S7e) and the nitrate/ΔCO ratio continued to rise after afternoon peak, especially after the evening rush hours (Fig. S7a). The continuously increase in the nitrate/ΔCO ratio before midnight could be contributed by the enhanced nocturnal N_2O_5 heterogeneous uptake reactions (Sun et al., 2018; Wang et al., 2017). Thus, the result may suggest that the primary pollutants and precursors emitted from traffic sources largely contributed to the marked evening peak of NR-PM_1 concentrations.

3.3.3. Variation of chemical composition on SLB days

During SLB days, NR-PM_1 concentrations were 2 times higher within SB periods (12.5 μg m^{-3}) than LB periods (6.4 μg m^{-3}). The chemical composition of NR-PM_1 varied significantly from LB to SB, especially for sulfate and MO-OOA (Fig. 5). The fraction of sulfate evidently decreased from 26.4% in LB periods to 19.8% in SB periods. Many studies revealed that sulfate was effectively formed through the cloudy and aqueous chemistry (Harris et al., 2013; Seinfeld and Pandis, 2016), and the elevated sulfate during the day was probably caused by strong transport and advection in the afternoon (Cao et al., 2017; Massimi et al., 2022; Salcedo et al., 2006). In this study, the high sulfate fraction in LB periods was contributed by enhanced aqueous-phase reactions favored by high RH at night (1:00–8:00, Fig. 3c). On the other hand, SLB is a mesoscale local circulation, thus on SLB days, the transport unlikely contributed much to sulfate during the daytime (i.e. SB periods) as mentioned above.

As shown in Fig. S8, the concentration of MO-OOA increased the most among all the chemical composition during the SB periods compared to LB periods. The fraction of MO-OOA increased from 15.5% in LB periods to 21.1% in SB periods, while the fraction of LO-OOA remained comparable between the two periods (Fig. 5). The previous studies had shown that the dominant formation pathway of LO-OOA was photochemical reaction (Hu et al., 2016; Xu et al., 2017), but the high O_x condition was favorable for the further conversion of LO-OOA to MO-OOA (Sun et al., 2011; Zhan et al., 2021). The later and broader peak of the MO-OOA/ΔCO than that of the LO-OOA/ΔCO also suggests the conversion of LO-OOA to MO-OOA on SLB days with high O_x (Fig. S7h, i). The remarkable increase of MO-OOA in SB periods was likely explained by efficient oxidation of POA and LO-OOA under SLB circulatory conditions. This result was expected because of the strong UV and low RH environment (Fig. 3c, d) during SLB-SB period favorable for photochemical processes and aerosol aging due to air mass retention.

3.4. Evolution of a SLB case

To further investigate the influence of SLB circulation on aerosols, we compared a SLB case and a non-SLB case in detail (Fig. 6). A two-consecutive-SLB-days case occurred on Nov. 26–27, with the wind direction transformed evidently between the land breeze and sea breeze. As one class of non-SLB cases, a local pollution case (LP case) that occurred during Dec. 11–12 was chosen in this study. The wind in the LP case came from the sea in the period 13:00–20:00, similar to the SLB case, but the wind in the LP case was quite still in the period 1:00–8:00. On the whole, the average wind speed was 1.8 m s^{-1} for the LP case relative to 2.8 m s^{-1} for the SLB case, suggesting that both of the cases were local pollution events. The diurnal variations of meteorological parameters like *T*, RH, BLH, and UV were consistent for the two cases. However, the peak of *T*, BLH, UV, and the valley of RH during the daytime were more marked in the SLB case than the LP case, which is consistent with the discussion in section 3.2.

The LP case here had a higher average NO_2 concentration than the SLB case. As expected, there was an increase in NO_2 concentrations in the evening rush hours for both cases. However, continuously northeaster wind direction (LB) from the midnight to early morning in the SLB case was favor for the diffusion of NO_2. Whereas, the still wind in the same period of the LP case mostly resulted in accumulation of NO_2 after it emitted from traffic sources. The afternoon peak of O_3 in the LP case

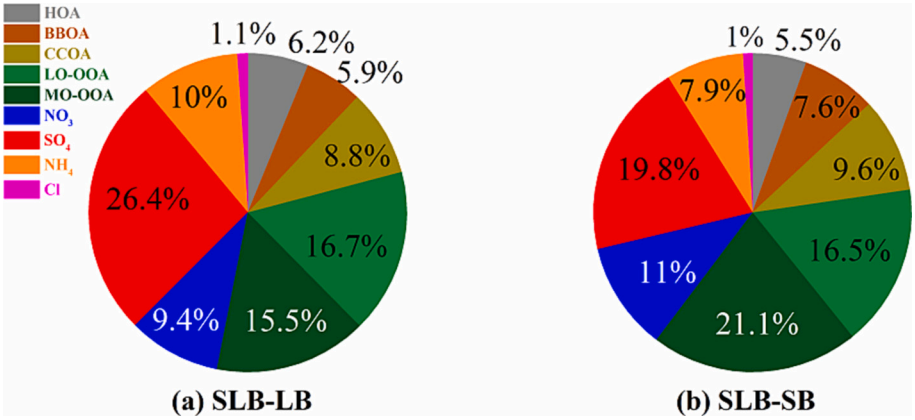

Fig. 5. The fraction of chemical composition in NR-PM_1 during (a) SLB-LB and (b) SLB-SB periods.

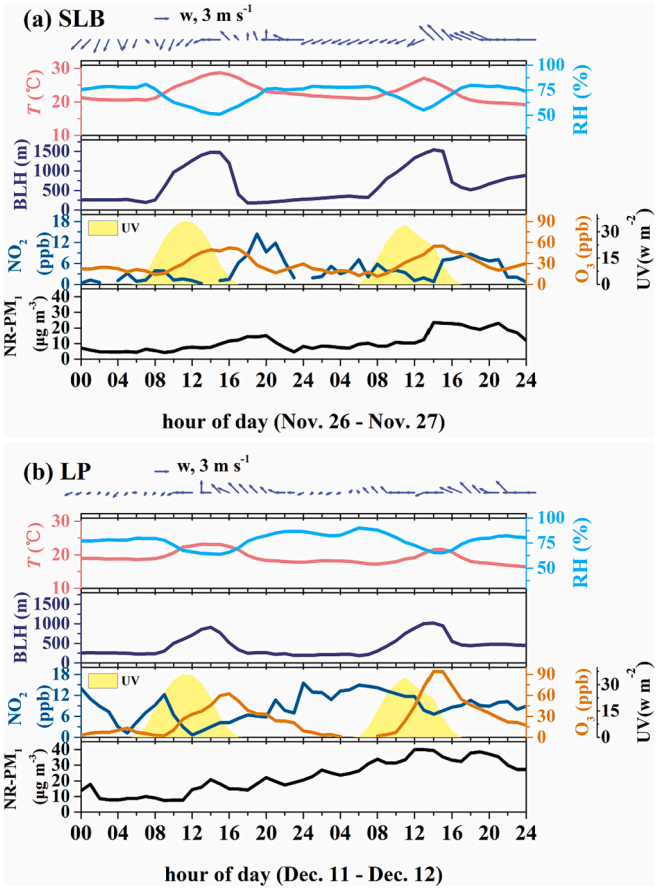

Fig. 6. Temporal variations of meteorological parameters, gaseous pollutants, and NR-PM_1 during (a) the SLB case, and (b) the LP case in 2020.

was more marked than that in the SLB case, especially for the second day of the LP case. The possible reason might be that the high level of NO_2 in the early morning of the LP case provided sufficient precursors for O_3 formation.

The average concentrations of NR-PM_1 were 22.5 μg m^{-3} for the LP case and 10.9 μg m^{-3} for the SLB case. In terms of chemical composition, the NR-PM_1 in the SLB case was characterized by a high fraction of OA (56.7%) and a low fraction of NO_3 (13.4%) compared to those in the LP case (46.7% and 30.6% for OA and NO_3, respectively). This result is well consistent with the general difference between SLB and non-SLB days discussed above. The whole variation trend of NR-PM_1 concentrations and its chemical composition was significantly different between the two cases (Fig. 7). For the LP case, the NR-PM_1 concentrations rose continuously (Fig. 7b). The contribution of NO_3 elevated most obviously with the increase of NR-PM_1. The large fraction of NO_3 reaching 40% appeared from the evening of the first day to the morning of the second day. More abundant precursor NO_2 and the lower T and higher RH during the night of the LP case enhanced the formation and the partitioning of nitrate from gas to particulate phase, resulting in the continuous increase of NO_3.

Unlike the LP case, the diurnal variations of NR-PM_1 for the two days of the SLB case were nearly duplicated, with a low level in the early morning, an upward trend during the day, and a peak in the late evening (Fig. 7a). The NR-PM_1 concentration on the second day was nearly twice of that on the first day. Note that the concentrations of chemical composition in the SLB case increased in the comparable pace on the second day compared to the first day. The extremely large fraction of OA in NR-PM_1 in the SLB case was mainly contributed by OOA. As shown in Fig. 7c, the fraction of LO-OOA in NR-PM_1 was relatively stable an entire day, but the fraction of MO-OOA obviously elevated at midday, indicating that the enhanced photochemical formation of MO-OOA during the daytime. The NO_3 fraction in the SLB case increased distinctly in the evening, especially during the second day. It was mainly caused by the synergistic contributions of sufficient precursors emitted by traffic in the evening rush hours, the shallow boundary layer, and likely cyclic amplification, according to the above discussion. Studies on both observations and simulations implied that increased stability caused by aerosol-PBL interaction might continue to affect the atmospheric stratification and aggravate the pollution on the next day (Huang et al., 2018). Additionally, the air mass was blown to the ocean by LB, spent several hours in the marine environment, and then was carried back to the land by SB. Thus, the successive SLB circulations would result in multiple accumulations of pollutants.

4. Conclusion

This study investigated the characteristics of meteorology, air pollutants, and NR-PM_1 chemical composition under the influence of SLB in a coastal city of Southeast China. The diurnal variations of meteorological parameters were similar between SLB and non-SLB days, but the day-night difference in T, RH, BLH, and UV was larger on SLB days. The diurnal variation of air pollutants, especially NO_2 and NR-PM_1 on SLB days showed an outstanding peak in the late evening, which was likely the combination results of pollutant emissions during the evening rush hours, the sharp reduction of BLH, and the air circulation driven by the daily LB/SB reversals. In addition, the late evening peak of NR-PM_1 was also contributed by secondary formation with large precursor NO_2 emissions.

Compared to non-SLB days, the fraction of OOA in NR-PM_1 increased

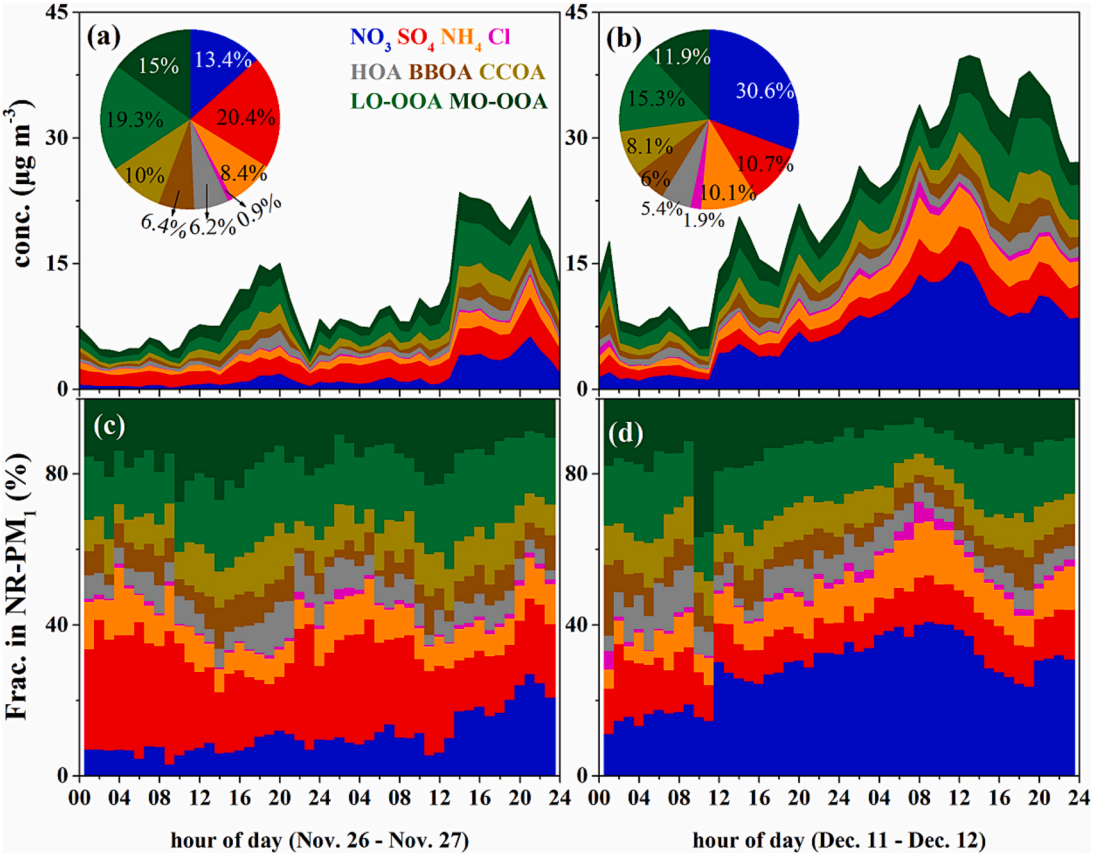

Fig. 7. Temporal variations of mass concentrations and chemical composition of NR-PM_1 during (a,c) the SLB case, and (b,d) the LP case in 2020.

and the fraction of NO_3 decreased significantly on SLB days. SLB days were characterized by strong photochemical indicators such as UV and O_x during the daytime, which enhanced the photochemical formation of OOA. Moreover, the elevated fraction of sulfate during the LB period was likely due to nocturnal aqueous-phase reaction formation, while the elevated fraction of MO-OOA during the SB period was mainly ascribed to the favorable environment for photochemical processes and aerosol aging. Cases study further highlighted that, compared with LP case, the NR-PM_1 in SLB case was characterized by elevated fraction of OOA, and the successive SLB circulations would result in the cyclic amplification of air pollutants. Our results provide a plausible explanation for the evolution of atmospheric aerosol chemistry and atmospheric pollution processes in coastal cities.

CRediT authorship contribution statement

Yuping Chen: Conceptualization, Methodology, Software, Investigation, Writing – review & editing. **Chen Yang:** Conceptualization, Writing – review & editing. **Lingling Xu:** Conceptualization, Writing – review & editing. **Xiaolong Fan:** Investigation, Writing – review & editing. **Jiayan Shi:** Visualization. **Ronghua Zheng:** Data curation. **Youwei Hong:** Investigation. **Mengren Li:** Investigation. **Taotao Liu:** Investigation. **Gaojie Chen:** Data curation. **Liqian Yin:** Data curation. **Jinsheng Chen:** Conceptualization, Supervision, Writing – review & editing.

Declaration of Competing Interest

The authors declare that they have no known competing financial interests or personal relationships that could have appeared to influence the work reported in this paper.

Data availability

Data will be made available on request.

Acknowledgements

This study was funded by the Natural Science Foundation of Fujian Province (2022 L3025 and 2021 J01528), the Cultivating Project of Strategic Priority Research Program of Chinese Academy of Sciences (XDPB19003), the National Key Research and Development Program (2022YFC3700304), the National Natural Science Foundation of China (U22A20578), the Center for Excellence in Regional Atmospheric Environment, CAS (E0L1B20201), Fujian Key Laboratory of Atmospheric Ozone Pollution Prevention (Institute of Urban Environment, Chinese Academy of Sciences), and Xiamen Atmospheric Environment Observation and Research Station of Fujian Province (Institute of Urban Environment, Chinese Academy of Sciences).

Appendix A. Supplementary data

Supplementary data to this article can be found online at https://doi.org/10.1016/j.atmosres.2023.106626.

References

An, Z., Huang, R.J., Zhang, R., Tie, X., Li, G., Cao, J., Zhou, W., Shi, Z., Han, Y., Gu, Z., Ji, Y., 2019. Severe haze in northern China: a synergy of anthropogenic emissions and atmospheric processes. Proc. Natl. Acad. Sci. 116 (18), 8657–8666. https://doi.org/10.1073/pnas.1900125116.

Augustin, P., Billet, S., Crumeyrolle, S., Deboudt, K., Dieudonné, E., Flament, P., Fourmentin, M., Guilbaud, S., Hanoune, B., Landkocz, Y., Méausoone, C., Roy, S., Schmitt, F.G., Sentchev, A., Sokolov, A., 2020. Impact of Sea Breeze Dynamics on Atmospheric Pollutants and their Toxicity in Industrial and Urban Coastal Environments. Remote Sens. 12 (4) https://doi.org/10.3390/rs12040648.

Bellouin, N., Quaas, J., Gryspeerdt, E., Kinne, S., Stier, P., Watson-Parris, D., Boucher, O., Carslaw, K.S., Christensen, M., Daniau, A.-L., Dufresne, J.-L., Feingold, G., Fiedler, S., Forster, P., Gettelman, A., Haywood, J.M., Lohmann, U., Malavelle, F., Mauritsen, T., McCoy, D.T., Myhre, G., Mülmenstädt, J., Neubauer, D., Possner, A., Rugenstein, M., Sato, Y., Schulz, M., Schwartz, S.E., Sourdeval, O., Storelvmo, T., Tolli, V., Winker, D., Stevens, B., 2020. Bounding global aerosol radiative forcing of climate change. Rev. Geophys. 58 (1) https://doi.org/10.1029/2019RG000660.

Berman, S., Ku, J.Y., Rao, S.T., 1999. Spatial and temporal variation in the mixing depth over the northeastern United States during the summer of 1995. J. Appl. Meteorol. 38 (12), 1661–1673. https://doi.org/10.1175/1520-0450(1999)038<1661:Satvit>2.0.Co;2.

Borne, K., Chen, D., Nunez, M., 1998. A method for finding sea breeze days under stable synoptic conditions and its application to the swedish west coast. Int. J. Climatol. 18, 901–914. https://doi.org/10.1002/(SICI)1097-0088(19980630)18:8<901::AID-JOC295>3.0.CO;2-F.

Canagaratna, M.R., Jayne, J.T., Jimenez, J.L., Allan, J.D., Alfarra, M.R., Zhang, Q., Onasch, T.B., Drewnick, F., Coe, H., Middlebrook, A., Delia, A., Williams, L.R., Trimborn, A.M., Northway, M.J., DeCarlo, P.F., Kolb, C.E., Davidovits, P., Worsnop, D.R., 2007. Chemical and microphysical characterization of ambient aerosols with the aerodyne aerosol mass spectrometer. Mass Spectrom. Rev. 26 (2), 185–222. https://doi.org/10.1002/mas.20115.

Canonaco, F., Crippa, M., Slowik, J.G., Baltensperger, U., Prévôt, A.S.H., 2013. SoFi, an IGOR-based interface for the efficient use of the generalized multilinear engine (ME-2) for the source apportionment: ME-2 application to aerosol mass spectrometer data. Atmosph. Measure. Tech. 6 (12), 3649–3661. https://doi.org/10.5194/amt-6-3649-2013.

Cao, L., Zhu, Q., Huang, X., Deng, J., Chen, J., Hong, Y., Xu, L., He, L., 2017. Chemical characterization and source apportionment of atmospheric submicron particles on the western coast of Taiwan Strait, China. J. Environ. Sci. 52, 293–304. https://doi.org/10.1016/j.jes.2016.09.018.

Cass, G.R., Shair, F.H., 1984. Sulfate accumulation in a sea breeze/land breeze circulation system. J. Geophys. Res. 89, 1429–1438. https://doi.org/10.1029/JD089iD01p01429.

Chen, T., Liu, J., Ma, Q., Chu, B., Zhang, P., Ma, J., Liu, Y., Zhong, C., Liu, P., Wang, Y., Mu, Y., He, H., 2021. Measurement report: Effects of photochemical aging on the formation and evolution of summertime secondary aerosol in Beijing. Atmos. Chem. Phys. 21 (2), 1341–1356. https://doi.org/10.5194/acp-21-1341-2021.

Chen, Y., Yang, C., Xu, L., Chen, J., Zhang, Y., Shi, J., Fan, X., Zheng, R., Hong, Y., Li, M., 2022. Chemical composition of NR-PM_1 in a coastal city of Southeast China: temporal variations and formation pathways. Atmos. Environ. 285 https://doi.org/10.1016/j.atmosenv.2022.119243.

Cohen, A.J., Brauer, M., Burnett, R., Anderson, H.R., Frostad, J., Estep, K., Balakrishnan, K., Brunekreef, B., Dandona, L., Dandona, R., Feigin, V., Freedman, G., Hubbell, B., Jobling, A., Kan, H., Knibbs, L., Liu, Y., Martin, R., Morawska, L., Pope, C.A., Shin, H., Straif, K., Shaddick, G., Thomas, M., van Dingenen, R., van Donkelaar, A., Vos, T., Murray, C.J.L., Forouzanfar, M.H., 2017. Estimates and 25-year trends of the global burden of disease attributable to ambient air pollution: an analysis of data from the Global Burden of Diseases Study 2015. Lancet 389 (10082), 1907–1918. https://doi.org/10.1016/s0140-6736(17)30505-6.

Di Bernardino, A., Iannarelli, A.M., Casadio, S., Mevi, G., Campanelli, M., Casasanta, G., Cede, A., Tiefengraber, M., Siani, A.M., Spinei, E., Cacciani, M., 2021. On the effect of sea breeze regime on aerosols and gases properties in the urban area of Rome, Italy. Urban Clim. 37 https://doi.org/10.1016/j.uclim.2021.100842.

Ding, A., Wang, T., Zhao, M., Wang, T., Li, Z., 2004. Simulation of sea-land breezes and a discussion of their implications on the transport of air pollution during a multi-day ozone episode in the Pearl River Delta of China. Atmos. Environ. 38 (39), 6737–6750. https://doi.org/10.1016/j.atmosenv.2004.09.017.

Furberg, M., Steyn, D.G., Baldi, M., 2002. The climatology of sea breezes on Sardinia. Int. J. Climatol. 22 (8), 917–932. https://doi.org/10.1002/joc.780.

Gahmberg, M., Savijärvi, H., Leskinen, M., 2010. The influence of synoptic scale flow on sea breeze induced surface winds and calm zones. Tellus A: Dynam. Meteorol. Oceanograph. 62 (2), 209–217. https://doi.org/10.1111/j.1600-0870.2009.00423.x.

Harris, E., Sinha, B., van Pinxteren, D., Tilgner, A., Fomba, K.W., Schneider, J., Roth, A., Gnauk, T., Fahlbusch, B., Mertes, S., Lee, T., Collett, J., Foley, S., Borrmann, S., Hoppe, P., Herrmann, H., 2013. Enhanced role of transition metal ion catalysis during in-cloud oxidation of SO_2. Science 340 (6133), 727–730. https://doi.org/10.1126/science.1230911.

Herndon, S.C., Onasch, T.B., Wood, E.C., Kroll, J.H., Canagaratna, M.R., Jayne, J.T., Zavala, M.A., Knighton, W.B., Mazzoleni, C., Dubey, M.K., Ulbrich, I.M., Jimenez, J. L., Seila, R., de Gouw, J.A., de Foy, B., Fast, J., Molina, L.T., Kolb, C.E., Worsnop, D. R., 2008. Correlation of secondary organic aerosol with odd oxygen in Mexico City. Geophys. Res. Lett. 35 (15) https://doi.org/10.1029/2008gl034058.

Hu, W., Hu, M., Hu, W., Jimenez, J.L., Yuan, B., Chen, W., Wang, M., Wu, Y., Chen, C., Wang, Z., Peng, J., Zeng, L., Shao, M., 2016. Chemical composition, sources, and aging process of submicron aerosols in Beijing: Contrast between summer and winter. J. Geophys. Res. Atmos. 121 (4), 1955–1977. https://doi.org/10.1002/2015jd024020.

Hu, W., Hu, M., Hu, W.-W., Zheng, J., Chen, C., Wu, Y., Guo, S., 2017. Seasonal variations in high time-resolved chemical composition, sources, and evolution of atmospheric submicron aerosols in the megacity Beijing. Atmos. Chem. Phys. 17 (16), 9979–10000. https://doi.org/10.5194/acp-17-9979-2017.

Huang, J.-P., Fung, J.C.H., Lau, A.K.H., 2006. Integrated processes analysis and systematic meteorological classification of ozone episodes in Hong Kong. J. Geophys. Res. 111 (D20) https://doi.org/10.1029/2005jd007012.

Huang, X., Wang, Z., Ding, A., 2018. Impact of Aerosol-PBL interaction on haze pollution: multiyear observational evidences in North China. Geophys. Res. Lett. 45 (16), 8596–8603. https://doi.org/10.1029/2018gl079239.

Jeffreys, H., 1922. On the dynamics of wind. Q. J. R. Meteorol. Soc. 48, 29–46.

Lee, B.P., Li, Y.J., Yu, J.Z., Louie, P.K.K., Chan, C.K., 2013. Physical and chemical characterization of ambient aerosol by HR-ToF-AMS at a suburban site in Hong Kong during springtime 2011. J. Geophys. Res. Atmos. 118 (15), 8625–8639. https://doi.org/10.1002/jgrd.50658.

Lelieveld, J., Evans, J.S., Fnais, M., Giannadaki, D., Pozzer, A., 2015. The contribution of outdoor air pollution sources to premature mortality on a global scale. Nature 525 (7569), 367–371. https://doi.org/10.1038/nature15371.

Liu, H., Chan, J.C.L., 2002. An investigation of air-pollutant patterns under sea-land breezes during a severe air-pollution episode in Hong Kong. Atmos. Environ. 36, 591–601. https://doi.org/10.1016/S1352-2310(01)00504-0.

Liu, W., Zhang, Q., Li, C., Xu, L., Xiao, W., 2022. The influence of soil moisture on convective activity: a review. Theor. Appl. Climatol. https://doi.org/10.1007/s00704-022-04046-z.

Lo, J.C.F., Lau, A.K.H., Fung, J.C.H., Chen, F., 2006. Investigation of enhanced cross-city transport and trapping of air pollutants by coastal and urban land-sea breeze circulations. J. Geophys. Res. 111, D14104. https://doi.org/10.1029/2005JD006837.

Masselink, G., Pattiaratchi, C.B., 1998. The effect of sea breeze on beach morphology, surf zone hydrodynamics and sediment resuspension. Mar. Geol. 146, 115–135. https://doi.org/10.1016/S0025-3227(97)00121-7.

Massimi, L., Pietrodangelo, A., Frezzini, M.A., Ristorini, M., De Francesco, N., Sargolini, T., Amoroso, A., Di Giosa, A., Canepari, S., Perrino, C., 2022. Effects of COVID-19 lockdown on PM_{10} composition and sources in the Rome Area (Italy) by elements' chemical fractionation-based source apportionment. Atmos. Res. 266 https://doi.org/10.1016/j.atmosres.2021.105970.

Miao, J.-E., Yang, M.-J., 2020. A modeling study of the severe afternoon thunderstorm event at Taipei on 14 June 2015: the roles of Sea Breeze, Microphysics, and Terrain. J. Meteorol. Soc. Jpn. 98 (1), 129–152. https://doi.org/10.2151/jmsj.2020-008.

Middlebrook, A.M., Bahreini, R., Jimenez, J.L., Canagaratna, M.R., 2012. Evaluation of composition-dependent collection efficiencies for the aerodyne aerosol mass spectrometer using field data. Aerosol Sci. Technol. 46 (3), 258–271. https://doi.org/10.1080/02786826.2011.620041.

Miller, S.T.K., Keim, B.D., Talbot, R.W., Mao, H., 2003. Sea breeze: structure, forecasting, and impacts. Rev. Geophys. 41 (3) https://doi.org/10.1029/2003rg000124.

Ng, N.L., Herndon, S.C., Trimborn, A., Canagaratna, M.R., Croteau, P.L., Onasch, T.B., Sueper, D., Worsnop, D.R., Zhang, Q., Sun, Y.L., Jayne, J.T., 2011. An aerosol chemical speciation monitor (ACSM) for routine monitoring of the composition and mass concentrations of Ambient Aerosol. Aerosol Sci. Technol. 45 (7), 780–794. https://doi.org/10.1080/02786826.2011.560211.

Paasonen, P., Asmi, A., Petäjä, T., Kajos, M.K., Äijälä, M., Junninen, H., Holst, T., Abbatt, J.P.D., Arneth, A., Birmili, W., van der Gon, H.D., Hamed, A., Hoffer, A., Laakso, L., Laaksonen, A., Richard Leaitch, W., Plass-Dülmer, C., Pryor, S.C., Räisänen, P., Swietlicki, E., Wiedensohler, A., Worsnop, D.R., Kerminen, V.-M., Kulmala, M., 2013. Warming-induced increase in aerosol number concentration likely to moderate climate change. Nat. Geosci. 6 (6), 438–442. https://doi.org/10.1038/ngeo1800.

Papanastasiou, D.K., Melas, D., 2009. Climatology and impact on air quality of sea breeze in an urban coastal environment. Int. J. Climatol. 29 (2), 305–315. https://doi.org/10.1002/joc.1707.

Salcedo, D., Onasch, T.B., Dzepina, K., Canagaratna, M.R., Zhang, Q., Huffman, J.A., DeCarlo, P.F., Jayne, J.T., Mortimer, P., Worsnop, D.R., Kolb, C.E., Johnson, K.S., Zuberi, B., Marr, L.C., Volkamer, R., Molina, L.T., Molina, M.J., Cardenas, B., Bernabe, R.M., Marquez, C., Gaffney, J.S., Marley, N.A., Laskin, A., Shutthanandan, V., Xie, Y., Brune, W., Lesher, R., Shirley, T., Jimenez, J.L., 2006. Characterization of ambient aerosols in Mexico City during the MCMA-2003 campaign with Aerosol Mass Spectrometry: results from the CENICA Supersite. Atmos. Chem. Phys. 6, 925–946. https://doi.org/10.5194/acp-6-925-2006.

Seinfeld, J.H., Pandis, S.N., 2016. Atmospheric Chemistry and Physics: From Air Pollution to Climate Change. John Wiley & Sons, New York.

Shen, X., Lee, T., Guo, J., Wang, X., Li, P., Xu, P., Wang, Y., Ren, Y., Wang, W., Wang, T., Li, Y., Carn, S.A., Collett, J.L., 2012. Aqueous phase sulfate production in clouds in eastern China. Atmos. Environ. 62, 502–511. https://doi.org/10.1016/j.atmosenv.2012.07.079.

Shiraiwa, M., Ueda, K., Pozzer, A., Lammel, G., Kampf, C.J., Fushimi, A., Enami, S., Arangio, A.M., Frohlich-Nowoisky, J., Fujitani, Y., Furuyama, A., Lakey, P.S.J., Lelieveld, J., Lucas, K., Morino, Y., Poschl, U., Takahama, S., Takami, A., Tong, H., Weber, B., Yoshino, A., Sato, K., 2017. Aerosol health effects from molecular to global scales. Environ. Sci. Technol. 51 (23), 13545–13567. https://doi.org/10.1021/acs.est.7b04417.

Sun, Y., Zhang, Q., Schwab, J., Chen, W., Bae, M., Lin, Y., Hung, H., Demerjian, K., 2011. A case study of aerosol processing and evolution in summer in New York City. Atmos. Chem. Phys. 11 (24), 12737–12750. https://doi.org/10.5194/acp-11-12737-2011.

Sun, Y., Wang, Z., Dong, H., Yang, T., Li, J., Pan, X., Chen, P., Jayne, J.T., 2012. Characterization of summer organic and inorganic aerosols in Beijing, China with an Aerosol Chemical Speciation Monitor. Atmos. Environ. 51, 250–259. https://doi.org/10.1016/j.atmosenv.2012.01.013.

Sun, Y., Du, W., Wang, Q., Zhang, Q., Chen, C., Chen, Y., Chen, Z., Fu, P., Wang, Z., Gao, Z., Worsnop, D.R., 2015. Real-time characterization of aerosol particle composition above the Urban Canopy in Beijing: insights into the interactions between the atmospheric boundary layer and aerosol chemistry. Environ. Sci. Technol. 49 (19), 11340–11347. https://doi.org/10.1021/acs.est.5b02373.

Sun, Y., Du, W., Fu, P., Wang, Q., Li, J., Ge, X., Zhang, Q., Zhu, C., Ren, L., Xu, W., Zhao, J., Han, T., Worsnop, D.R., Wang, Z., 2016. Primary and secondary aerosols in Beijing in winter: sources, variations and processes. Atmos. Chem. Phys. 16 (13), 8309–8329. https://doi.org/10.5194/acp-16-8309-2016.

Sun, Y., Xu, W., Zhang, Q., Jiang, Q., Canonaco, F., Prévôt, A.S.H., Fu, P., Li, J., Jayne, J., Worsnop, D.R., Wang, Z., 2018. Source apportionment of organic aerosol from 2-year highly time-resolved measurements by an aerosol chemical speciation monitor in Beijing, China. Atmos. Chem. Phys. 18 (12), 8469–8489. https://doi.org/10.5194/acp-18-8469-2018.

Tsai, H.H., Yuan, C.S., Hung, C.H., Lin, C., Lin, Y.C., 2011. Influence of sea-land breezes on the tempospatial distribution of atmospheric aerosols over coastal region. Air & Waste Manage. Assoc. 61 (4), 358–376. https://doi.org/10.3155/1047-3289.61.4.358.

Wagner, N.L., Riedel, T.P., Roberts, J.M., Thornton, J.A., Angevine, W.M., Williams, E.J., Lerner, B.M., Vlasenko, A., Li, S.M., Dubé, W.P., Coffman, D.J., Bon, D.M., de Gouw, J.A., Kuster, W.C., Gilman, J.B., Brown, S.S., 2012. The sea breeze/land breeze circulation in Los Angeles and its influence on nitryl chloride production in this region. J. Geophys. Res. Atmos. 117 (D21) https://doi.org/10.1029/2012jd017810. D00V24.

Wang, Y.C., Huang, R.J., Ni, H.Y., Chen, Y., Wang, Q.Y., Li, G.H., Tie, X.X., Shen, Z.X., Huang, Y., Liu, S.X., Dong, W.M., Xue, P., Fröhlich, R., Canonaco, F., Elser, M., Daellenbach, K.R., Bozzetti, C., El Haddad, I., Prévôt, A.S.H., Canagaratna, M.R., Worsnop, D.R., Cao, J.J., 2017. Chemical composition, sources and secondary processes of aerosols in Baoji city of Northwest China. Atmos. Environ. 158, 128–137. https://doi.org/10.1016/j.atmosenv.2017.03.026.

Xu, W., Han, T., Du, W., Wang, Q., Chen, C., Zhao, J., Zhang, Y., Li, J., Fu, P., Wang, Z., Worsnop, D.R., Sun, Y., 2017. Effects of Aqueous-phase and photochemical processing on secondary organic aerosol Formation and evolution in Beijing, China. Environ. Sci. Technol. 51 (2), 762–770. https://doi.org/10.1021/acs.est.6b04498.

Yang, H., Wang, J., Chen, M., Nie, D., Shen, F., Lei, Y., Ge, P., Gu, T., Gai, X., Huang, X., Ma, Q., 2020. Chemical characteristics, sources and evolution processes of fine particles in Lin'an, Yangtze River Delta, China. Chemosphere 254, 126851. https://doi.org/10.1016/j.chemosphere.2020.126851.

Yang, T., Wang, H., Li, H., Guo, X., Wang, D., Chen, X., Wang, F., Xin, J., Sun, Y., Wang, Z., 2022. Quantitative attribution of wintertime haze in coastal East China to local emission and regional intrusion under a stagnant internal boundary layer. Atmos. Environ. 276 https://doi.org/10.1016/j.atmosenv.2022.119006.

Zhan, B., Zhong, H., Chen, H., Chen, Y., Li, X., Wang, L., Wang, X., Mu, Y., Huang, R.-J., George, C., Chen, J., 2021. The roles of aqueous-phase chemistry and photochemical oxidation in oxygenated organic aerosols formation. Atmos. Environ. 266 https://doi.org/10.1016/j.atmosenv.2021.118738.

Zhao, W., Fan, S., Guo, H., Gao, B., Sun, J., Chen, L., 2016. Assessing the impact of local meteorological variables on surface ozone in Hong Kong during 2000–2015 using quantile and multiple line regression models. Atmos. Environ. 144, 182–193. https://doi.org/10.1016/j.atmosenv.2016.08.077.

Zhao, J., Du, W., Zhang, Y., Wang, Q., Chen, C., Xu, W., Han, T., Wang, Y., Fu, P., Wang, Z., Li, Z., Sun, Y., 2017. Insights into aerosol chemistry during the 2015 China Victory Day parade: results from simultaneous measurements at ground level and 260 m in Beijing. Atmos. Chem. Phys. 17 (4), 3215–3232. https://doi.org/10.5194/acp-17-3215-2017.

Zhao, Q., Huo, J., Yang, X., Fu, Q., Duan, Y., Liu, Y., Lin, Y., Zhang, Q., 2020. Chemical characterization and source identification of submicron aerosols from a year-long real-time observation at a rural site of Shanghai using an Aerosol Chemical Speciation Monitor. Atmos. Res. 246 https://doi.org/10.1016/j.atmosres.2020.105154.

Zhou, W., Xu, W., Kim, H., Zhang, Q., Fu, P., Worsnop, D.R., Sun, Y., 2020. A review of aerosol chemistry in Asia: insights from aerosol mass spectrometer measurements. Environ Sci Process Impacts 22 (8), 1616–1653. https://doi.org/10.1039/d0em00212g.